RSC Advances

PAPER

Cite this: *RSC Adv.*, 2015, **5**, 94615

Nitrogen-doped graphene/carbon nanotube/Co_3O_4 hybrids: one-step synthesis and superior electrocatalytic activity for the oxygen reduction reaction†

Hengyi Lu,[a] Yunpeng Huang,[a] Jiajie Yan,[a] Wei Fan*[b] and Tianxi Liu*[ab]

Received 1st September 2015
Accepted 23rd October 2015

DOI: 10.1039/c5ra17759f

www.rsc.org/advances

Oxygen reduction reaction (ORR) catalysts play an important role in fuel cells, and the ever-increasing energy demand calls for efficient and cost-effective ORR catalysts. However, commercial ORR catalysts are mainly noble metal based materials like Pt/C, which suffer from drawbacks of high cost and poor stability. In this study, we prepared a non-noble metal ORR catalyst with high efficiency through a simple one-step hydrothermal method, in which the reduction of graphene oxide (GO) along with the doping of nitrogen and Co_3O_4 nanoparticles were realized at the same time, thus resulting in a unique hierarchical structure of nitrogen-doped reduced graphene oxide/carbon nanotube/Co_3O_4 (N-rGO/CNT/Co_3O_4) hybrids. Due to the synergistic effects between the active components and the effective nitrogen doping, as well as the space effect of CNTs and Co_3O_4 nanoparticles on avoiding the restacking of graphene nanosheets, the N-rGO/CNT/Co_3O_4 hybrids exhibited enhanced ORR catalytic performance with long-term stability and excellent resistance towards methanol crossover effects, indicating their promising potential as ORR electrocatalysts in practical applications.

1. Introduction

Electrochemical energy conversion/storage systems like supercapacitors, lithium ion batteries and fuel cells (FCs) are promising solutions for the upcoming energy crisis and severe environmental issues.[1] Among them, FCs have drawn more and more attention since they can convert the chemical energy of fuels, *i.e.* hydrogen or methanol, into electricity at high efficiency (40–60%, even 85% when waste heat was used) without any emission of toxic by-products.[1–3] However, the sluggish cathode oxygen reduction reaction (ORR) greatly limits the efficiency of FCs in the practical applications.[1] For this reason, high performance ORR catalysts are indispensable to improve the efficiency of FCs. Up to now, commercial ORR catalysts are still Pt-based materials which suffer from high cost, low durability and great crossover effects.[4] In recent years, some non-noble metal catalysts like carbon-based materials,[5–7] transition metal oxides (TMOs),[8,9] transition metal chalcogenides[10] are emerging as a promising replacement of Pt-based catalysts for ORR due to their low cost and high performance.

TMOs, especially Co_3O_4, have been intensively investigated recently due to their relatively good ORR catalytic activities and earth-abundant feature.[9] However, when used as ORR catalyst alone, the catalytic performance of pure TMOs is greatly compromised by their poor conductivity, dissolution and agglomeration. One promising way to solve this problem is to hybridize them with carbon-based supporting materials like graphene,[11,12] carbon nanotubes (CNTs)[13,14] or porous carbon.[15] For instance, Co_3O_4 nanoparticles were grown on mildly oxidized graphene oxide as a highly active and long-term stable catalyst for both ORR and oxygen evolution reaction (OER). And it was found that the possible formation of interfacial Co–O–C and Co–N–C bonds may be the reason for the synergistic ORR catalytic activity.[11] Nitrogen doped mesoporous graphene was also been utilized as supporting materials for the immobilization of Co_3O_4.[16] The pores in graphene sheets are favorable for the easy access to reactants and allow rapid charge transfer during the reaction, thus yielding a high performance ORR catalyst. Therefore, developing appropriate supporting material may be the key challenge for developing high performance ORR catalysts.

Carbon materials with unique physicochemical properties are ideal supporting materials for TMO loading in order to improve their electrocatalytic activity. Among various carbon materials, one-dimensional (1D) CNTs and two-dimensional (2D) graphene are proved to be promising ORR catalysts or

[a]*State Key Laboratory of Molecular Engineering of Polymers, Department of Macromolecular Science, Fudan University, 220 Handan Road, Shanghai 200433, P. R. China. E-mail: txliu@fudan.edu.cn; Fax: +86-21-65640293; Tel: +86-21-55664197*
[b]*State Key Laboratory of Modification of Chemical Fibers and Polymer Materials, College of Materials Science and Engineering, Donghua University, 2999 North Renmin Road, Shanghai 201620, P. R. China. E-mail: 10110440003@fudan.edu.cn*

† Electronic supplementary information (ESI) available. See DOI: 10.1039/c5ra17759f

catalyst carriers owing to their intrinsic excellent conductivity, large specific surface area and corrosion resistance.[17] However, CNTs and graphene tend to restack or aggregate due to the strong van der Waals interaction between individual CNTs and graphene sheets, which seriously decreases its large surface area and electrochemical active sites, and largely limits their practical application.[18,19] Hence, many efforts have been devoted to solve the above problems by constructing various graphene/CNT hybrids. For example, Wei *et al.*[20] prepared a nitrogen-doped graphene/single-walled CNT hybrid in which CNTs were vertically grown on the surface of graphene as efficient bi-functional catalyst for ORR and OER through an *in situ* chemical vapor deposition (CVD) method. Yang *et al.*[21] prepared a CNT-doped graphene hybrid (G–CNT) through a long time hydrothermal process followed by a thermal treatment under Ar atmosphere. They claimed that the unusual high ORR activity was stemmed from the localized charge separation at the interface of graphene and CNTs, which is beneficial for oxygen adsorption. A kind of paper ORR catalyst were prepared by loading catalyst nanoparticles on free-standing GO/CNTs membrane.[22] Nevertheless, most of the previous work on graphene/CNT hybrids involved incorporation of surfactant that impairs the conductivity, or tedious preparation method such as CVD or high-temperature treatment. In this regard, our group has reported a simple and efficient approach to utilize GO as versatile dispersants to directly stabilize pristine CNTs in aqueous media through mild sonication.[23] In this GO/CNT hybrids thus prepared, 1D CNTs between 2D GO sheets could serve as spacers to prevent the restacking of graphene sheets during the reduction process. Additionally, CNTs could bridge individual GO sheets to form a three-dimensional (3D) interconnected network, thus providing effective transport channels for ion and electron. Therefore, graphene/CNT hybrids with 3D conductive framework and large specific surface area are promising supporting materials for further incorporation of nanoparticles to obtain enhanced ORR catalytic performance.

It is also worth noting that heteroatoms doping, such as nitrogen and sulfur, could significantly improve the ORR activity of graphene and CNTs.[24–26] On the one hand, nitrogen-doping could change the electronic and surface chemical properties of graphene or CNTs which benefits the absorption of oxygen molecules on the catalyst surface, thus enhances the $4e^-$ process of ORR. On the other hand, nitrogen sites could be anchoring sites for metal oxides *via* strong bonding between metal atoms and the carbon surface, which could help the dispersion of catalyst particles thus improve the activity of hybrids.[11,17,27] Different N-containing species like ammonia,[28] urea,[29] melamine,[24,30] pyrrole,[31,32] pyridine[33] and aniline[34] can be used to introduce heteroatoms into graphene or CNTs. For example, nitrogen-doped graphene was synthesized by introducing ammonia during the CVD process, which shows high activity and long-term stability as the ORR catalyst.[28]

Herein, we introduced a simple one-step hydrothermal method to prepare nitrogen-doped reduced graphene oxide/carbon nanotube/Co_3O_4 (N-rGO/CNT/Co_3O_4) hybrids, which were directly used as ORR catalysts. As illustrated in Scheme 1, CNTs were first added into GO suspension to form GO/CNT hybrids by sonication. Then, Co-precursor (cobalt acetate) and N-precursor (ammonia) were sequentially added into the suspension followed by a simple hydrothermal process. Interestingly, the formation of Co_3O_4 nanoparticles, reduction of GO and nitrogen-doping of graphene occurred simultaneously during the hydrothermal process. In addition, the whole preparation process does not involve any complex process like CVD or high temperature treatments. Electrochemical tests show that the obtained N-rGO/CNT/Co_3O_4 hybrids exhibit high catalytic activity for ORR in terms of superior stability and excellent tolerance to methanol crossover effects. The impressive performance was stemmed from the unique hybrid structures with synergistic effects of three active components. Firstly, highly conductive CNTs serving as both spacers and conductive linkers could prevent the restacking of graphene sheets and increase the overall conductivity of the hybrids. Secondly, nitrogen-doping is beneficial for the adsorption of oxygen molecules on the surface of catalyst, thus enhances the $4e^-$ process. Finally, the synergistic effects between uniformly dispersed Co_3O_4 nanoparticles and N-rGO/CNT hybrids could further improve the catalytic activity by providing numerous active sites and ion/electron transfer pathways. Therefore, the N-rGO/CNT/Co_3O_4 hybrids with enhanced ORR catalytic performance provide a promising alternative for the development of next-generation Pt-free fuel cell catalysts.

2. Experimental

2.1. Materials

Natural graphite powder (325 meshes) and commercial Pt/C catalyst (platinum, 20 wt% on carbon black) were purchased from Alfa Aesar. Multi-walled carbon nanotubes (95%, 20–50 nm in diameter; ~20 μm in length, produced by the CVD method) were obtained from Chengdu Organic Chemicals Co. Ltd. 98% H_2SO_4, 30% H_2O_2, 37% HCl, 25% NH_4OH, $NaNO_3$, *N*,*N*-dimethylformamide (DMF), $KMnO_4$, cobalt acetate ($Co(OAc)_2 \cdot 4H_2O$) were supplied by Sinopharm Chemical Reagent Co. Ltd and used without any further treatment.

2.2. Preparation of GO/CNT hybrid suspension

Graphite oxide was synthesized by the modified Hummers method.[35–38] GO suspension (1 mg mL^{-1}) was prepared by sonicating 200 mg graphite oxide in 200 mL deionized water for 2 h. Then, a stable GO/CNT hybrid suspension was prepared according to our previously reported work.[23] Briefly, 50 mg pristine CNTs were directly added into 100 mL 1 mg mL^{-1} GO suspension, followed by sonication for 2 h. The stable GO/CNT hybrid suspension was obtained after removing the unstable CNTs by centrifugation at 8000 rpm (RCF = 4650, TGL-18C-C, ShangHai Anting Scientific Instrument Factory) for 5 min. The mass ratio of GO and CNTs in the suspension was 2 : 1.

2.3. Preparation of N-rGO/CNT/Co_3O_4 hybrids

N-rGO/CNT/Co_3O_4 hybrids were synthesized by a simple one-step hydrothermal reaction. In a typical process, certain amounts of $Co(OAc)_2 \cdot 4H_2O$ were dissolved in 2 mL DI water.

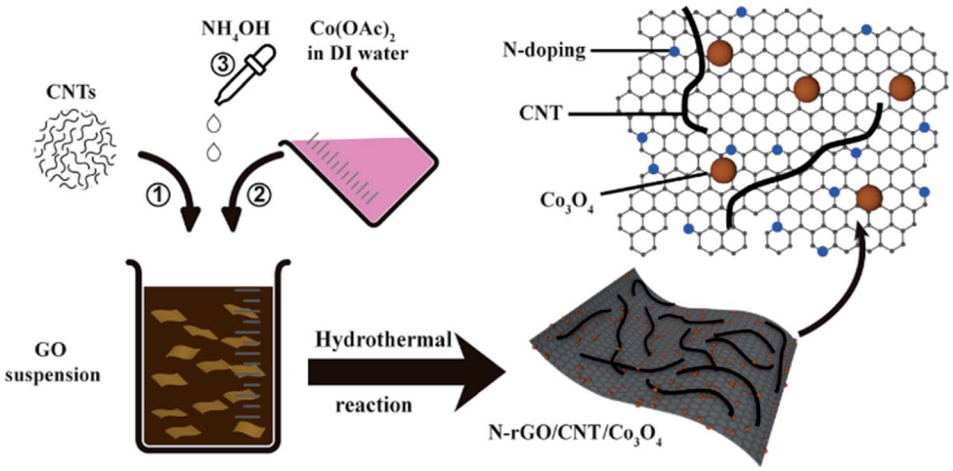

Scheme 1 The preparation process of N-rGO/CNT/Co_3O_4 hybrids.

Then the solution was added dropwise into 20 mL 1.5 mg mL^{-1} stable GO/CNT hybrid suspension. After sonicating for 30 min, 2 mL 25% NH_4OH was added into the above dispersion under vigorous stirring for 10 min before transferring into a 50 mL Teflon autoclave. After hydrothermal reaction at 150 °C for 3 h, the black precipitate was collected by centrifugation and washed with DI water for three times. The final product was dried at 60 °C for 12 h and directly used as ORR catalyst without any further treatments. The hybrids obtained from different amounts of $Co(OAc)_2 \cdot 4H_2O$ (0.025 mmol, 0.05 mmol, 0.1 mmol, 0.2 mmol) are denoted as N-rGO/CNT/0.025 Co_3O_4, N-rGO/CNT/0.05 Co_3O_4, N-rGO/CNT/0.1 Co_3O_4 and N-rGO/CNT/0.2 Co_3O_4, respectively. For comparison, N-rGO/CNT and rGO/CNT binary hybrids were also prepared under the same conditions without adding $Co(OAc)_2 \cdot 4H_2O$ or both $Co(OAc)_2 \cdot 4H_2O$ and NH_4OH.

2.4. Characterization

Transmission electron microscopy (TEM) observation was conducted on a Philip CM300 FEG TEM instrument under an accelerating voltage of 200 kV. Field emission scanning electron microscopy (FESEM) images were obtained on a JSM-6700F SEM at an accelerating voltage of 5 kV. X-ray diffraction (XRD) measurements were carried out using a PANalytical X'pert PRO XRD with Cu Kα radiation (λ = 0.1542 nm; operating voltage, 40 kV; cathode current, 40 mA; scan rate, 5° min^{-1}). X-ray photoelectron spectroscopy (XPS) spectra were collected by a Phoibos 100 spectrometer with a monochromatic Mg X-ray radiation source. Thermo-gravimetric analysis (Pyris 1 TGA) was carried out in air with a heating rate of 5 °C min^{-1} from 100 °C to 800 °C.

2.5. Electrochemical measurements

All electrochemical measurements were carried out on a CHI 660D electrochemical workstation (Shanghai Chenhua Equipments, China). 4 mg of catalyst was first dispersed in 1 mL mixed solvent of 500 μL DMF, 490 μL H_2O and 10 μL Nafion (5%) under sonication. Then 2.5 μL and 5 μL above suspension was respectively deposited onto polished glassy carbon electrode (GCE, d = 3 mm, Shanghai Chenhua Equipments, China) and glassy carbon rotating-disk electrode (RDE, d = 5 mm, 616A, Princeton Applied Research) followed by drying at room temperature. The electrochemical tests were conducted in a conventional three-electrode cell in O_2 (or N_2) saturated 0.1 M KOH aqueous solution at room temperature by using Ag/AgCl as reference electrode, and Pt wire as counter electrode. The scan rate was 5 mV s^{-1} for cyclic voltammetry (CV) measurements and RDE measurements. All data were recorded after the shapes of CV curves were stable in N_2 saturated 0.1 M KOH. Linear sweep voltammetry (LSV) measurements were carried out at different rotating speed from 400 rpm to 2025 rpm in the O_2 saturated 0.1 M KOH solution. The Koutecky–Levich (K–L) equation was used to calculate the electron transfer number:

$$\frac{1}{J} = \frac{1}{J_k} + \frac{1}{J_l} = \frac{1}{J_k} + \frac{1}{B\omega^{0.5}} \quad (1)$$

$$B = 0.2nF(D_0)^{2/3}v^{-1/6}C_0 \quad (2)$$

where J is the measured current density, J_k is the kinetic-limiting current density, J_l is the diffusion-limiting current density, ω is the electrode rotation rate (rpm), n is the electron transfer number in ORR, F is the Faraday constant (96 485C mol^{-1}), D_0 is the diffusion coefficient of O_2 in 0.1 M KOH solution (1.9×10^{-5} cm^2 s^{-1}), C_0 is the bulk concentration of O_2 (1.2×10^{-6} mol cm^{-3}), and v is the velocity of the electrolyte (0.01 cm^2 s^{-1}). The constant 0.2 is used when the rotation rate is expressed in rpm.

3. Results and discussion

3.1. Morphology and structure of N-rGO/CNT/Co_3O_4 hybrids

As well known, pristine CNTs cannot form stable suspension in aqueous medium which greatly limits its wide applications. However, GO aqueous suspension is very stable due to the presence of hydrophilic groups such as hydroxyl, carboxyl, and epoxy groups on the surface and edges of GO. In our previous

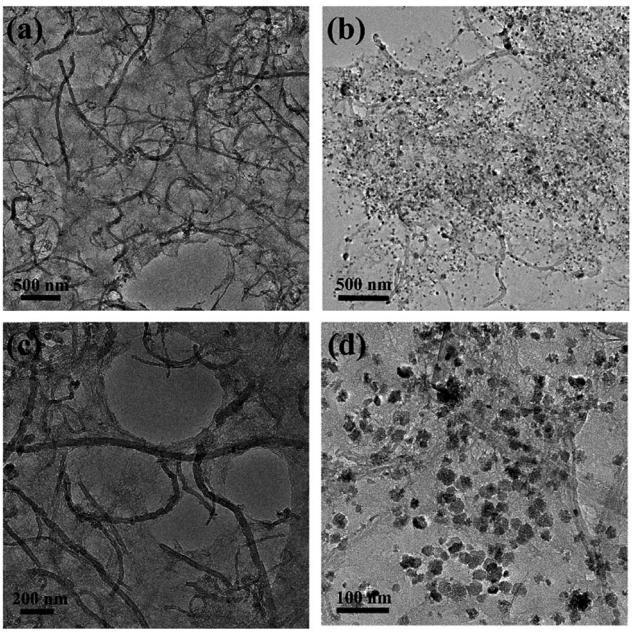

Fig. 1 TEM images of (a and c) GO/CNT and (b and d) N-rGO/CNT/0.05 Co_3O_4 hybrids at low (top) and high (down) magnifications.

work, we found that GO could act as excellent dispersant to help the dispersion of CNTs in aqueous solution.[23] After simple sonicating the mixture of pristine CNTs and GO, a stable suspension of GO/CNT hybrids can be readily obtained when the mass ratio of GO and CNTs was controlled in a proper range. It is reasonable to suppose that the π-conjugated multiple aromatic regions of GO sheets could interact with the sidewalls of CNTs through the π-stacking interaction, while the hydrophilic oxygen groups maintain the water dispersibility of the GO/CNT hybrids.[23] As shown by the TEM image in Fig. 1a and c, well-defined configuration of GO/CNT hybrids can be clearly observed, in which hair-like CNTs were randomly yet uniformly distributed on the surface of GO sheets without any aggregation. It is well known that there are lots of defects on GO sheets obtained by the modified Hummers method, which cannot be fully restored even after being reduced to graphene (rGO) and these defects are harmful to the conductivity of the hybrids. However, pristine CNTs on the surface of GO could interconnect with each other to form conductive networks, thus greatly increase the conductivity of the hybrids, especially when the mass ratio of GO/CNTs is 2 : 1.[39] As for the preparation of N-rGO/CNT/Co_3O_4 hybrids, Co-precursor (cobalt acetate) and N-precursor (ammonia) were sequentially added into the GO/CNT hybrid suspension followed by a simple one-step hydrothermal process, where the formation of Co_3O_4 nanoparticles, reduction of GO and nitrogen-doping of graphene occurred simultaneously. Successful growth of Co_3O_4 is confirmed by TEM observation (Fig. 1b and d), nano-sized (10–20 nm) Co_3O_4 particles were uniformly grown on both the surface of rGO and CNTs, indicating that N-rGO/CNT hybrid is a suitable substrate to help the dispersion of Co_3O_4 nanoparticles.

Fig. 2a shows XRD patterns of GO/CNT, N-rGO/CNT and N-rGO/CNT/0.05 Co_3O_4 hybrids. As can be seen, two peaks of GO/CNT hybrid at $2\theta = 10.6°$ (d-spacing = 7.6 Å) and 26.1° (d-spacing = 3.4 Å) correspond to the d-spacing of GO and CNTs, respectively. Compared to GO/CNT hybrid, N-rGO/CNT hybrid has only one peak at $2\theta = 26.1°$, which suggests that GO has been reduced to rGO successfully after the hydrothermal process. A series of sharp peaks of N-rGO/CNT/0.05 Co_3O_4 hybrid correspond to the (111), (220), (311), (222), (400), (422), (511) and (440) crystal facets of Co_3O_4, showing the good crystalline structure of Co_3O_4 nanoparticles. The peak at $2\theta = 26.1°$ corresponding to rGO/CNT hybrid disappears for N-rGO/CNT/0.05 Co_3O_4 hybrid since the peak intensity of Co_3O_4 is much higher than those of carbon materials. The XRD results prove that the growth of Co_3O_4 nanoparticles and the reduction of GO were successfully implemented after hydrothermal reaction. XPS characterization was performed to determine the elemental composition of rGO/CNT and N-rGO/CNT/0.05 Co_3O_4 hybrids (Fig. 2b–d). In the N-rGO/CNT/0.05 Co_3O_4 hybrid, the content of C, O, N, Co elements were 80.3 at%, 12.8 at%, 4.8 at% and 2.1 at%, respectively. The presence of N 1s peak in the spectrum of N-rGO/CNT/Co_3O_4 hybrid as compared to rGO/CNT hybrid confirms the successful doping of nitrogen. The content of nitrogen element in N-rGO/CNT/0.05 Co_3O_4 hybrid was 4.8 at%. High-resolution N 1s spectrum reveals that nitrogen atoms exist three states, including pyridinic N (398.7 eV), pyrrolic N (400.0 eV) and graphitic N (401.3 eV). Both pyridinic N and pyrrolic N locate at the edges of graphene planes, yet pyrrolic N could contribute two p-electron to the π-system while pyridinic N only contributes one p-electron, thus pyrrolic N has higher binding energy than pyridinic N. Graphitic N refers to those nitrogen atoms doped into graphene planes by substituting the carbon atoms in hexagonal rings.[16,30,40] Previous studies reported that pyridinic N could lower the onset potential of ORR and the graphitic N determines the limiting current density,[40,41] thus the nitrogen-doping in N-rGO/CNT/Co_3O_4 hybrids could

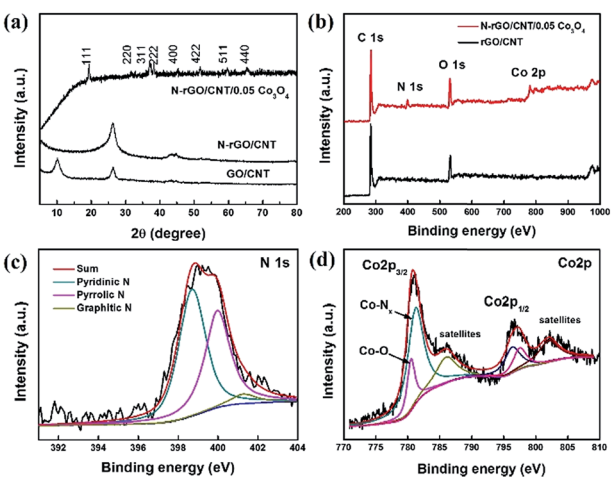

Fig. 2 (a) XRD patterns of GO/CNT, N-rGO/CNT and N-rGO/CNT/0.05 Co_3O_4 hybrids. (b) Survey XPS spectra of rGO/CNT and N-rGO/CNT/0.05 Co_3O_4 hybrids. High resolution (c) N 1s spectrum and (d) Co 2p spectrum.

contribute to the improved ORR performance. Besides, as mentioned above, the nitrogen-doping sites could be the anchoring center for the metal oxides, which may be the reason for the good dispersion and relative small size of the Co_3O_4 nanoparticles. The Co 2p spectrum of N-rGO/CNT/0.05 Co_3O_4 hybrid show two main peaks at 796.7 eV and 780.7 eV, respectively assigned to Co $2p_{1/2}$ and Co $2p_{3/2}$, and there are two weak satellite peak besides the main peak, which further confirms the formation of Co_3O_4. The peak deconvolution of Co $2p_{3/2}$ suggests two peaks at 779.6 eV and 781.2 eV, which respectively correspond to Co–O and Co–N_x bonds.[42] These results confirm that after the simple one-step hydrothermal reaction, N-rGO/CNT/Co_3O_4 hybrids were successfully obtained and the hybridization between the carbon materials, nitrogen and Co_3O_4 were realized.

To optimize the composition of the ternary hybrids, N-rGO/CNT/Co_3O_4 hybrids with different contents of Co_3O_4 were prepared. As shown in Fig. 3, all the hybrids exhibit porous structures without any aggregation of CNTs, and Co_3O_4 nanoparticles are uniformly dispersed on the surface of N-rGO/CNT substrate. This structure clearly indicates that the CNTs can prevent the restacking of graphene sheets during the reduction process and interconnect together to form conductive network. When the content of Co_3O_4 increases, the size of Co_3O_4 nanoparticles decreases and they start to form clusters (Fig. 3d). This may result in the decrease of the active contact area between Co_3O_4 nanoparticles and the electrolyte.

3.2. Electrochemical evaluation of ORR performance

Cyclic voltammetry (CV) was first utilized to assess the electrochemical ORR activity of rGO/CNT, N-rGO/CNT and N-rGO/CNT/Co_3O_4 hybrids in O_2 or N_2 saturated 0.1 M KOH with the same mass loading (Fig. S1†). All the samples only show well-defined cathodic reduction peaks in the presence of O_2. Fig. 4 compares the performance of each hybrid in a more intuitive way. Generally, more positive peak potential and larger peak current mean higher catalytic activity. It is clear that pure Co_3O_4 nanoparticles exhibit very poor ORR activity with a peak potential at −0.40 V. Both rGO/CNT and N-rGO/CNT hybrids show more positive peak and larger peak current than pure Co_3O_4, and N-rGO/CNT hybrid exhibits a higher peak potential (−0.19 V) than rGO/CNT hybrid (−0.22 V), indicating that nitrogen-doping can enhance the catalytic activity of rGO/CNT hybrid. When Co_3O_4 is incorporated into the hybrid, the highest peak potential (−0.15 V) and peak current are obtained, which is due to the synergistic effect of Co_3O_4 and N-rGO/CNT hybrid. This phenomenon can be explained by that the bonding between Co_3O_4 and N-rGO could change the chemical bonding environment for C, O, Co atoms, and the Co–O–C and Co–N–C bonds may be the active center for ORR.[11,43] When the loading content of Co_3O_4 varies, the peak position of N-rGO/CNT/Co_3O_4 hybrids does not show obvious shift while the peak current greatly changes, presenting a rising followed by downward trend with increasing the Co_3O_4 content. The possible reason is that too much Co_3O_4 will cause aggregation of nanoparticles (Fig. 3d), thus lower the available surface area and impede the reactants from adsorbing onto the active sites.[44] The most active sample is N-rGO/CNT/0.05 Co_3O_4 hybrid which performs a comparable activity to commercial Pt/C catalyst. The content of Co_3O_4 in this hybrid is 19.2% by mass as calculated from the TGA data (Fig. S2†). In this regard, the following tests will be conducted with the N-rGO/CNT/0.05 Co_3O_4 hybrid unless explicitly noted.

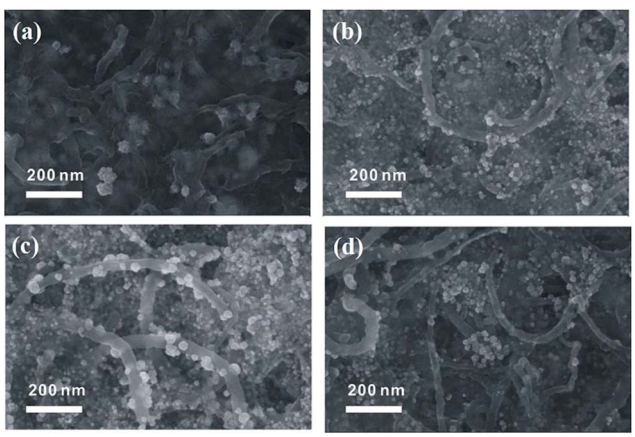

Fig. 3 FESEM images of N-rGO/CNT/Co_3O_4 hybrids with different Co_3O_4 contents. (a) N-rGO/CNT/0.025 Co_3O_4, (b) N-rGO/CNT/0.05 Co_3O_4, (c) N-rGO/CNT/0.1 Co_3O_4, and (d) N-rGO/CNT/0.2 Co_3O_4.

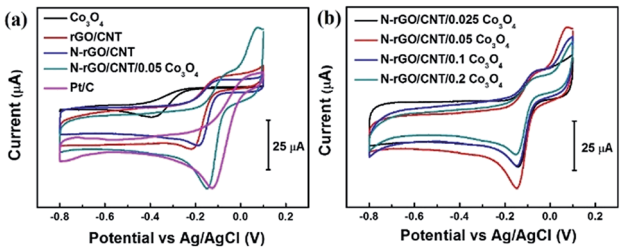

Fig. 4 CV curves of different samples in O_2 saturated 0.1 M KOH solution.

In order to further evaluate the electrocatalytic activity and reveal the kinetics of the hybrids prepared, linear sweep voltammetry (LSV) measurements were performed in O_2 saturated 0.1 M KOH at a scan rate of 5 mV s^{-1}. Fig. 5a shows a series of LSV curves of N-rGO/CNT/0.05 Co_3O_4 hybrids on the rotating disk electrode (RDE) at different rotation rates from 400 rpm to 2025 rpm. The current density increases sharply in the mixed kinetic-diffusion control region (about −0.1 V to −0.3 V), indicating the fast diffusion of reactants on the hybrid catalysts, which is attributed to the porous structure generated by CNTs. The Koutecky–Levich (K–L) plots were created according to eqn (1) and (2) at different potentials. The corresponding K–L plots of N-rGO/CNT/0.05 Co_3O_4 hybrid (Fig. 5b) show a good linearity and near parallelism at different potentials, indicating that the ORR process catalyzed by the hybrid obeys the first-order reaction kinetics with respect to the concentration of dissolved oxygen. The electron transfer number calculated from the K–L plots at −0.4 to −0.7 V for N-rGO/CNT/0.05 Co_3O_4 hybrid is

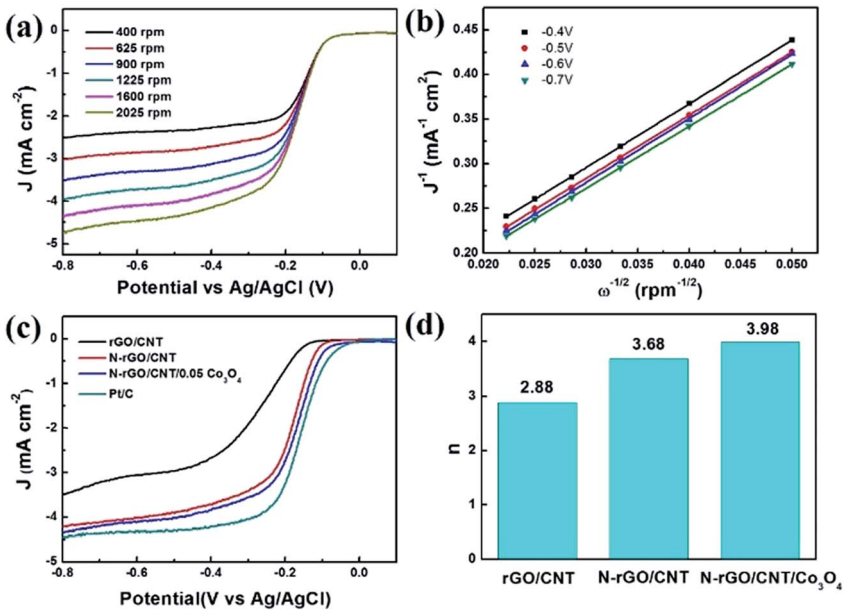

Fig. 5 (a) RDE voltammograms of N-rGO/CNT/0.05 Co_3O_4 hybrid in O_2 saturated 0.1 M KOH at rotation rates from 400 rpm to 2025 rpm. (b) K–L plots of the N-rGO/CNT/0.05 Co_3O_4 hybrid. (c) RDE voltammograms of different samples in O_2 saturated 0.1 M KOH at rotation rate of 1600 rpm. (d) Electron transfer number of different hybrids.

about 3.98, suggesting that the hybrid favors a direct $4e^-$ oxygen reduction process.

The catalytic performance of N-rGO/CNT/Co_3O_4 hybrids was further compared with other samples. Here, the potential at which the ORR current density at 5% of the diffusion-limited current density was chosen as the onset potential.[45] As shown in Fig. 5c, the onset potential of N-rGO/CNT (−0.11 V) is much higher than that of rGO/CNT (−0.16 V), indicating that nitrogen-doping can facilitate the ORR activity. The electron transfer numbers of rGO/CNT and N-rGO/CNT hybrids were calculated from Fig. S3 and S4.† N-rGO/CNT hybrid has a higher electron transfer number ($n = 3.68$) than that ($n = 2.88$) of rGO/CNT hybrid. This is because, in addition to the electrons donated to the conjugated π bond, some nitrogen atoms with lone pair electrons could change the electrical properties of graphene and enhance the O_2 adsorption on the catalyst, thus could afford easier electron transfer between the catalyst and O_2 molecule and enhance the $4e^-$ process. When Co_3O_4 nanoparticles are introduced, a higher onset potential and a larger current density can be obtained. The onset potential of N-rGO/CNT/Co_3O_4 hybrids (−0.09 V) is close to that (−0.06 V) of commercial Pt/C catalyst, which once again proves the excellent catalytic performance of N-rGO/CNT/Co_3O_4 hybrids. Besides, the half-wave potentials of different samples have the same trend as the onset potential. The kinetic-limited current density of N-rGO/CNT/Co_3O_4 hybrids is calculated to be 14.16 mA cm^{-2}. As discussed above, pyridinic N could lower the onset potential while graphitic N determines the limiting current density. The low content of graphitic N (0.2 at%) in N-rGO/CNT/Co_3O_4 hybrid could be the reason for the lower limiting current density compared to Pt/C, which could be further improved through increasing the content of graphitic N. Moreover, the N-rGO/CNT/Co_3O_4 hybrids exhibit much enhanced electrocatalytic performance when compared with other works in the literatures (Table S1†).

Long-term stability is also an important property for practical fuel cell applications. The durability tests of N-rGO/CNT/Co_3O_4 hybrids and commercial Pt/C catalysts toward ORR were conducted through chronoamperometric measurements at −0.4 V in O_2 saturated 0.1 M KOH at a rotation speed of 1600 rpm. As shown in Fig. 6a, the relative current of Pt/C has a visual decline about 45% after 20 000 s, while N-rGO/CNT/Co_3O_4 hybrid has a smaller decrease less than 20%, indicating the good long-term

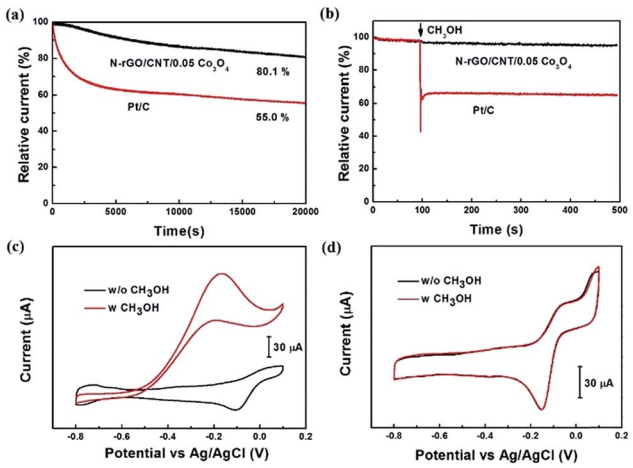

Fig. 6 Chronoamperometric responses of N-rGO/CNT/0.05 Co_3O_4 hybrid and Pt/C catalyst at −0.4 V (*vs.* Ag/AgCl) (a) in O_2 saturated 0.1 M KOH electrolyte, and (b) with the quick injection of methanol with a rotation rate of 1600 rpm. CV curves of (c) Pt/C and (d) N-rGO/CNT/0.05 Co_3O_4 hybrid before and after the addition of methanol.

stability of the hybrids. The possible reason is that the porous structure of the hybrids can suppress the structural collapse and active site dissolution, as well as enhance the contact of catalyst and oxygen. In fuel cells, there may exist fuel molecules penetrating through electrolyte membrane and contact with cathode catalysts, that is the so-called fuel crossover effects. To evaluate the tolerance of N-rGO/CNT/Co_3O_4 hybrids toward methanol crossover, current–time chronoamperometric measurements were recorded when methanol was introduced during the ORR process. As shown in Fig. 6b, the current response of N-rGO/CNT/Co_3O_4 hybrid remains unchanged while the Pt/C catalyst shows an instantaneous current jump upon addition of methanol. And the CV curves of N-rGO/CNT/Co_3O_4 hybrids before and after the addition of methanol remain almost the same, revealing the excellent tolerance to methanol crossover effects. Therefore, the N-rGO/CNT/Co_3O_4 hybrids exhibit excellent selectivity and durability, showing superior advantages over the commercial Pt/C when used as long-term running electrocatalysts.

4. Conclusions

In summary, a simple one-step hydrothermal method was developed to prepare ternary nitrogen-doped reduced graphene oxide/carbon nanotube/Co_3O_4 (N-rGO/CNT/Co_3O_4) hybrids, which exhibited comparable electrocatalytic ORR activity to commercial Pt/C catalyst with onset potential of −0.09 V (*vs.* Ag/AgCl), excellent tolerance to methanol crossover effects, and even better long-term stability. The possible reasons for the outstanding performance of the hybrids can be elaborated as follows. First, CNTs absorbed on GO sheets could prevent the restacking of graphene sheets during the reduction process and simultaneously form conductive network in the N-rGO/CNT/Co_3O_4 hybrids. In addition, nitrogen-doping could change the electronic properties of graphene, thus facilitating the absorption of O_2 on the surface of catalyst and enhancing the direct $4e^-$ process of ORR. Most importantly, by virtue of the mediation effects of N-rGO/CNT supporter on particle dispersion and size distribution, uniform incorporation of Co_3O_4 nanoparticles could provide numerous electrochemical active sites for efficient ORR process. Therefore, the low cost, simple and easy to scale-up preparation method, along with the excellent ORR performance make the N-rGO/CNT/Co_3O_4 hybrids promising non-precious ORR catalysts in fuel cell or metal–air battery applications.

Acknowledgements

The authors are grateful for the financial support from the National Natural Science Foundation of China (51125011, 51433001).

Notes and references

1 M. Winter and R. J. Brodd, *Chem. Rev.*, 2004, **104**, 4245–4270.
2 H. Choi, S. Jung, J. Seo, D. W. Chang, L. Dai and J. Baek, *Nano Energy*, 2012, **1**, 534–551.
3 M. Zhang and L. M. Dai, *Nano Energy*, 2012, **1**, 514–517.
4 Y. H. Bing, H. S. Liu, L. Zhang, D. Ghosh and J. J. Zhang, *Chem. Soc. Rev.*, 2010, **39**, 2184–2202.
5 H. Shi, Y. F. Shen, F. He, Y. Li, A. R. Liu, S. Q. Liu and Y. J. Zhang, *J. Mater. Chem. A*, 2014, **2**, 15704–15716.
6 H. Nie, Y. Zhang, W. Zhou, J. Li, B. Wu, T. Liu and H. Zhang, *Electrochim. Acta*, 2014, **150**, 205–210.
7 J. Li, Z. Li, J. Tong, C. Xia and F. Li, *RSC Adv.*, 2015, **5**, 70010–70016.
8 M. Sun, H. J. Liu, Y. Liu, J. H. Qu and J. H. Li, *Nanoscale*, 2012, **7**, 1250–1269.
9 G. Wu and P. Zelenay, *Acc. Chem. Res.*, 2013, **46**, 1878–1889.
10 M. R. Gao, J. Jiang and S. H. Yu, *Small*, 2012, **8**, 13–27.
11 Y. Y. Liang, Y. G. Li, H. L. Wang, J. G. Zhou, J. Wang, T. Regier and H. J. Dai, *Nat. Mater.*, 2011, **10**, 780–786.
12 X. G. Duan, Z. M. Ao, H. Q. Sun, S. Indrawirawan, Y. X. Wang, J. Kang, F. L. Liang, Z. H. Zhu and S. B. Wang, *ACS Appl. Mater. Interfaces*, 2015, **7**, 4169–4178.
13 Y. L. Liu, D. C. Higgins, J. Wu, M. Fowler and Z. W. Chen, *Electrochem. Commun.*, 2013, **34**, 125–129.
14 Y. Yao, B. Q. Zhang, J. Y. Shi and Q. H. Yang, *ACS Appl. Mater. Interfaces*, 2015, **7**, 7413–7420.
15 C. Zhang, M. Antonietti and T. Fellinger, *Adv. Funct. Mater.*, 2014, **24**, 7655–7665.
16 J. J. Xiao, X. J. Bian, L. Liao, S. Zhang, C. Ji and B. H. Liu, *ACS Appl. Mater. Interfaces*, 2014, **6**, 17654–17660.
17 L. M. Dai, D. W. Chang, J. B. Baek and W. Lu, *Small*, 2012, **8**, 1130–1166.
18 Y. Gao, G. Zong, H. Bai and Q. Fu, *Chin. J. Polym. Sci.*, 2014, **32**, 245–254.
19 C. H. Choi, M. W. Chung, Y. J. Jun and S. I. Woo, *RSC Adv.*, 2013, **3**, 12417–12422.
20 G. L. Tian, M. Q. Zhao, D. S. Yu, X. Y. Kong, J. Q. Huang, Q. Zhang and F. Wei, *Small*, 2014, **10**, 2251–2259.
21 W. Wei, Y. Tao, W. Lv, F. Y. Su, L. Ke, J. Li, D. W. Wang, B. H. Li, F. Y. Kang and Q. H. Yang, *Sci. Rep.*, 2014, **4**, 6289.
22 S. S. Li, H. P. Cong, P. Wang and S. H. Yu, *Nanoscale*, 2014, **6**, 7534–7541.
23 C. Zhang, L. L. Ren, X. Y. Wang and T. X. Liu, *J. Phys. Chem. C*, 2010, **114**, 11435–11440.
24 J. Liang, Y. Jiao, M. Jaroniec and S. Z. Qiao, *Angew. Chem., Int. Ed.*, 2012, **51**, 11496–11500.
25 Y. P. Zhu, Y. L. Liu, Y. P. Liu, T. Z. Ren, G. H. Du, T. H. Chen and Z. Y. Yuan, *J. Mater. Chem. A*, 2015, **3**, 11725–11729.
26 G. Jo, J. Sanetuntikul and S. Shanmugam, *RSC Adv.*, 2015, **5**, 53637–53643.
27 J. Wang, J. G. Zhou, Y. F. Hu and T. Regier, *Energy Environ. Sci.*, 2013, **6**, 926–934.
28 L. T. Qu, Y. Liu, J. B. Baek and L. M. Dai, *ACS Nano*, 2010, **4**, 1321–1326.
29 Z. Y. Lin, G. Waller, Y. Liu, M. L. Liu and C. P. Wong, *Adv. Energy Mater.*, 2012, **2**, 884–888.
30 Z. H. Sheng, L. Shao, J. J. Chen, W. J. Bao, F. B. Wang and X. H. Xia, *ACS Nano*, 2011, **5**, 4350–4358.
31 Y. Zhao, C. G. Hu, L. Song, L. X. Wang, G. Q. Shi, L. M. Dai and L. T. Qu, *Energy Environ. Sci.*, 2014, **7**, 1913–1918.
32 H. Wei, M. Xu, S. Bao, F. Yang and H. Chai, *RSC Adv.*, 2014, **4**, 16979–16984.

33 Q. Guo, D. Zhao, S. Liu, S. Chen, M. Hanif and H. Hou, *Electrochim. Acta*, 2014, **138**, 318–324.
34 M. K. Liu, Y. F. Song, S. X. He, W. W. Tjiu, J. S. Pan, Y. Y. Xia and T. X. Liu, *ACS Appl. Mater. Interfaces*, 2014, **6**, 4214–4222.
35 D. Li, M. B. Muller, S. Gilje, R. B. Kaner and G. G. Wallace, *Nat. Nanotechnol.*, 2008, **3**, 101–105.
36 N. I. Kovtyukhova, P. J. Ollivier, B. R. Martin, T. E. Mallouk, S. A. Chizhik, E. V. Buzaneva and A. D. Gorchinskiy, *Chem. Mater.*, 1999, **11**, 771–778.
37 C. Zhang, W. W. Tjiu, W. Fan, S. Huang and T. Liu, *J. Mater. Chem.*, 2012, **22**, 11748–11754.
38 Z. Wang, X. Tang, Z. Yu, P. Guo, H. Song and X. Duc, *Chin. J. Polym. Sci.*, 2011, **29**, 368–376.
39 C. Zhang, W. W. Tjiu and T. X. Liu, *Polym. Chem.*, 2013, **4**, 5785–5792.
40 T. Sharifi, G. Z. Hu, X. E. Jia and T. Wågberg, *ACS Nano*, 2012, **6**, 8904–8912.
41 L. F. Lai, J. R. Potts, D. Zhan, L. Wang, C. K. Poh, C. H. Tang, H. Gong, Z. X. Shen, J. Y. Lin and R. S. Ruoff, *Energy Environ. Sci.*, 2012, **5**, 7936–7942.
42 Y. Y. Jiang, Y. Z. Lu, X. D. Wang, Y. Bao, W. Chen and L. Niu, *Nanoscale*, 2014, **6**, 15066–15072.
43 C. W. Sun, F. Li, C. Ma, Y. Wang, Y. L. Ren, W. Yang, Z. H. Ma, J. Q. Li, Y. J. Chen, Y. Kim and L. Q. Chen, *J. Mater. Chem. A*, 2014, **2**, 7188–7196.
44 Y. Y. Liang, H. L. Wang, P. Diao, W. Chang, G. S. Hong, Y. G. Li, M. Gong, L. M. Xie, J. G. Zhou, J. Wang, T. Z. Regier, F. Wei and H. J. Dai, *J. Am. Chem. Soc.*, 2012, **134**, 15849–15857.
45 X. J. Zhou, J. L. Qiao, L. Yang and J. J. Zhang, *Adv. Energy Mater.*, 2014, **4**, 1301523.